

DRAFT VERSION FEBRUARY 8, 2022

Typeset using L^AT_EX **preprint** style in AASTeX63

Pressure-Strain Interaction as the Energy Dissipation Estimate in Collisionless Plasma

YAN YANG,^{1,2} W.H. MATTHAEUS,¹ SOHOM ROY,¹ VADIM ROYTERTSHEYN,³ TULASI PARASHAR,⁴
RIDDHI BANDYOPADHYAY,⁵ AND MINPING WAN⁶

¹*Department of Physics and Astronomy, University of Delaware, Newark, DE 19716, USA*

²*Southern University of Science and Technology, Shenzhen, Guangdong 518055, China*

³*Space Science Institute, Boulder, CO 80301, USA*

⁴*School of Chemical and Physical Sciences, Victoria University of Wellington, Wellington 6012, New Zealand*

⁵*Department of Astrophysical Sciences, Princeton University, Princeton, NJ 08544, USA*

⁶*Guangdong Provincial Key Laboratory of Turbulence Research and Applications, Department of Mechanics and Aerospace Engineering, Southern University of Science and Technology, Shenzhen, Guangdong 518055, China*

ABSTRACT

The dissipative mechanism in weakly collisional plasma is a topic that pervades decades of studies without a consensus solution. We compare several energy dissipation estimates based on energy transfer processes in plasma turbulence and provide justification for the pressure-strain interaction as a direct estimate of the energy dissipation rate. The global and scale-by-scale energy balances are examined in 2.5D and 3D kinetic simulations. We show that the global internal energy increase and the temperature enhancement of each species are directly tracked by the pressure-strain interaction. The incompressible part of the pressure-strain interaction dominates over its compressive part in all simulations considered. The scale-by-scale energy balance is quantified by scale filtered Vlasov-Maxwell equations, a kinetic plasma approach, and the lag dependent von Kármán-Howarth equation, an approach based on fluid models. We find that the energy balance is exactly satisfied across all scales, but the lack of a well-defined inertial range influences the distribution of the energy budget among different terms in the inertial range. Therefore, the widespread use of the Yaglom relation to estimating dissipation rate is questionable in some cases, especially when the scale separation in the system is not clearly defined. In contrast, the pressure-strain interaction balances exactly the dissipation rate at kinetic scales regardless of the scale separation.

1. INTRODUCTION

The picture of turbulence cascade as developed by Taylor, von Kármán, Kolmogorov and others (Taylor 1938; de Kármán & Howarth 1938; Kolmogorov 1941a,b) describes energy transfer across scales from an energy-containing range, through an inertial range and into a dissipation range where fluctuations are converted into internal energy. This basic picture is readily adapted to magnetohydrodynamics (MHD) (Biskamp 2003), a magnetofluid model (Moffatt 1978) often applied as an approximation to low density high temperature cosmic plasmas (Parker 1979) such as the solar wind

(Breech et al. 2008). Recently there has been increasing interest in advancing descriptions of turbulence in more complex plasma models (Bowers & Li 2007; Parashar et al. 2009; Howes et al. 2011). In particular there is impetus to understand dissipation for kinetic plasmas in which the classical collisional approach becomes inapplicable, and therefore also inapplicable are standard closures that capture dissipation as empirical descriptions in terms of fluid scale variables. Fortunately instead of studying specific dissipative mechanisms at kinetic scales, such as wave-particle interactions (Hollweg 1986; Hollweg & Isenberg 2002; Gary & Saito 2003; Gary et al. 2008; Howes et al. 2008; Markovskii et al. 2006; He et al. 2015; Chandran et al. 2010), field-particle correlations (Klein & Howes 2016; Chen et al. 2019; Klein et al. 2020) or heating by coherent structures and reconnection (Dmitruk et al. 2004; Retinò et al. 2007; Sundkvist et al. 2007; Parashar et al. 2011; TenBarge & Howes 2013; Perri et al. 2012; He et al. 2018), an alternative strategy based on the energy transfer process is available. One can proceed by tracing available pathways that lead to deposition of internal (or thermal) energy. “Dissipation” here simply refers to a degradation of fluid scale and electromagnetic fluctuations into internal energy (Matthaeus et al. 2020). This increase in internal energy is eventually “thermalized” by collisions and entropy production (Pezzi et al. 2019a; Liang et al. 2019) but this irreversibility is not our focus here.

Different dissipation proxies based on the energy transfer process have been adapted to estimate the dissipation rate. A von Kármán-Howarth picture (de Kármán & Howarth 1938) of turbulent decay was extended for MHD (Hossain et al. 1995; Wan et al. 2012a), in which the global decay rate of energy is controlled by the von Kármán decay law at energy-containing scales (Wan et al. 2012a; Wu et al. 2013; Zank et al. 2017; Bandyopadhyay et al. 2018b,a; Bandyopadhyay et al. 2019). The energy dissipation rate is estimated by the energy decay rate. The energy loss at energy-containing scales, is then transferred across scales in the MHD inertial range. To obtain the inertial range energy transfer rate, the Yaglom relation (Politano & Pouquet 1998; Sorriso-Valvo et al. 2007; Stawarz et al. 2009; Coburn et al. 2015; Bandyopadhyay et al. 2018) and its extensions (Osman et al. 2011; Podesta 2008; Hadid et al. 2017; Andrés et al. 2019; Banerjee & Galtier 2013; Wan et al. 2009; Hellinger et al. 2018; Ferrand et al. 2019; Verdini et al. 2015) have been adapted, in which the energy dissipation rate is estimated by the energy transfer rate. The transferred energy ultimately goes into the internal energy reservoir, which is often evaluated by the rate of work done by the electric field on particles for species α , $\mathbf{j}_\alpha \cdot \mathbf{E}$ (Zenitani et al. 2011; Wan et al. 2012b, 2015; Chasapis et al. 2018a; Ergun et al. 2018; Phan et al. 2018; Lu et al. 2019; Vörös et al. 2019; Pongkitiwanichakul et al. 2021) and more recently by the pressure-strain interaction for species α , $-(\mathbf{P}_\alpha \cdot \nabla) \cdot \mathbf{u}_\alpha$ (Yang et al. 2017a,b; Yang 2019; Sitnov et al. 2018; Chasapis et al. 2018b; Zhong et al. 2019; Bandyopadhyay et al. 2020a; Jiang et al. 2021).

One observable feature is that the aforementioned dissipation rate estimates dominate at different scales. Two standard ways to disentangle the multi-scale properties in configuration space are scale filtering representations and lag dependent structure functions. Scale filter (Germano 1992) is based on real space coarse-graining at a specified length scale, which is widely used in Large Eddy Simulation computational methods (Meneveau & Katz 2000; Pope 2004), in analytical theory (Eyink 2003; Aluie 2013), and recently in promising applications to turbulence in plasma models (Yang et al. 2017a; Eyink 2018; Yang et al. 2019; Teaca et al. 2021; Cerri & Camporeale 2020; Camporeale et al. 2018). Structure functions such as the von Kármán-Howarth relation (de Kármán & Howarth 1938; Monin & Yaglom 1975), defined in terms of increments, have a long history in turbulence theory (Frisch 1995).

Here we are concerned with energy balance across scales, measured using the von Kármán-Howarth equation (Verdini et al. 2015; Hellinger et al. 2018; Ferrand et al. 2019; Adhikari et al. 2021) and filtered Vlasov-Maxwell equations (Yang et al. 2017a; Matthaeus et al. 2020). In both scale filtering and structure function representations, crucial elements are energy loss at large scales, energy flux in an intermediate range, and dissipation at small scales. So we compare corresponding scale filtered and structure function decompositions and clarify the relationship between energy dissipation estimates at different scales.

A number of studies have been devoted to investigate the multiplicity of dissipation rate estimates (Yang et al. 2019; Matthaeus et al. 2020; Zhou et al. 2021; Bandyopadhyay et al. 2020b, 2021; Pezzi et al. 2020). In this paper we specifically address the role of the pressure-strain interaction for species α , $-(\mathbf{P}_\alpha \cdot \nabla) \cdot \mathbf{u}_\alpha$, in two aspects. On the one hand, different pathways contributing to the global evolution of energies are traced, as used in (Pezzi et al. 2019b; Song et al. 2020; Du et al. 2018), which illustrates the difference between $-(\mathbf{P}_\alpha \cdot \nabla) \cdot \mathbf{u}_\alpha$ and $\mathbf{j}_\alpha \cdot \mathbf{E}$. On the other hand, the scale decomposition of these pathways is realized using the von Kármán-Howarth equation and filtered Vlasov-Maxwell equations, which illustrates the relationship among the von Kármán decay law, the Yaglom relation and $-(\mathbf{P}_\alpha \cdot \nabla) \cdot \mathbf{u}_\alpha$. We make a detailed comparison of these elements using kinetic plasma simulations. Major findings are: *first*, that the potential deficiencies of the Yaglom relation to estimating dissipation rate, especially for the turbulence without well defined inertial range, is exemplified; *second*, that energy balance across scales is found, even when the Yaglom relation and its subsidiary assumptions are not valid; *third*, that the quantitatively correct description of dissipation in kinetic plasma is that computed from the pressure-strain interaction.

2. THEORY AND METHOD

2.1. Energy Balance Equations

There are multiple forms of energy available for participation in energy transfer in collisionless plasma. These include: electromagnetic energy $E^m = (\mathbf{B}^2 + \mathbf{E}^2)/(8\pi)$, where \mathbf{B} and \mathbf{E} are magnetic and electric fields; fluid flow kinetic energy of species α $E_\alpha^f = \rho_\alpha \mathbf{u}_\alpha^2/2$, where ρ_α is the mass density and \mathbf{u}_α is the fluid velocity; and corresponding internal energy $E_\alpha^{th} = \frac{1}{2}m_\alpha \int (\mathbf{v} - \mathbf{u}_\alpha)^2 f_\alpha(\mathbf{x}, \mathbf{v}, t) d\mathbf{v}$, with mass m_α and velocity distribution function f_α . The first three moments of the Vlasov equation, in conjunction with the Maxwell equations, yield the time evolution of the energies:

$$\partial_t E_\alpha^f + \nabla \cdot (E_\alpha^f \mathbf{u}_\alpha + \mathbf{P}_\alpha \cdot \mathbf{u}_\alpha) = (\mathbf{P}_\alpha \cdot \nabla) \cdot \mathbf{u}_\alpha + \mathbf{j}_\alpha \cdot \mathbf{E}, \quad (1)$$

$$\partial_t E_\alpha^{th} + \nabla \cdot (E_\alpha^{th} \mathbf{u}_\alpha + \mathbf{h}_\alpha) = -(\mathbf{P}_\alpha \cdot \nabla) \cdot \mathbf{u}_\alpha, \quad (2)$$

$$\partial_t E^m + \frac{c}{4\pi} \nabla \cdot (\mathbf{E} \times \mathbf{B}) = -\mathbf{j} \cdot \mathbf{E}, \quad (3)$$

where the subscript $\alpha = e, i$ represents the species, \mathbf{P}_α is the pressure tensor, \mathbf{h}_α is the heat flux vector, $\mathbf{j} = \sum_\alpha \mathbf{j}_\alpha$ is the total electric current density, $\mathbf{j}_\alpha = n_\alpha q_\alpha \mathbf{u}_\alpha$ is the electric current density of species α , and n_α and q_α are the number density and the charge of species α , respectively. Note that the spatial transport terms (i.e., the second terms on the left hand side) are globally conservative and cancel out under certain boundary conditions, e.g., periodic.

From these equations, one can see the roles of several energy transfer pathways. For example, the electric work, $\mathbf{j}_\alpha \cdot \mathbf{E}$, exchanges electromagnetic energy with fluid flow energy for species α , while the pressure-strain interaction, $-(\mathbf{P}_\alpha \cdot \nabla) \cdot \mathbf{u}_\alpha$, represents the conversion between fluid flow and internal

energy for species α . The pressure-strain interaction can be further decomposed as

$$\langle -(\mathbf{P}_\alpha \cdot \nabla) \cdot \mathbf{u}_\alpha \rangle = \langle -p_\alpha \nabla \cdot \mathbf{u}_\alpha - \Pi_\alpha : \mathbf{D}_\alpha \rangle = p\theta_\alpha + PiD_\alpha, \quad (4)$$

where $\langle \dots \rangle$ denotes spatial average, $p_\alpha = P_{\alpha,ii}/3$, $\Pi_{\alpha,ij} = P_{\alpha,ij} - p_\alpha \delta_{ij}$, and $D_{\alpha,ij} = (\partial_i u_{\alpha,j} + \partial_j u_{\alpha,i})/2 - (\nabla \cdot \mathbf{u}_\alpha) \delta_{ij}/3$. $p\theta_\alpha$ and PiD_α denote compressible and incompressible parts respectively.

2.2. Scale Filtering Representation

To disentangle the scale-by-scale dynamics, it is useful to define a filter (Germano 1992) at scale ℓ , operating on the velocity and electromagnetic fields. With a properly defined filtering kernel $G_\ell(\mathbf{r}) = \ell^{-d} G(\mathbf{r}/\ell)$, where d is the spatial dimension and $G(\mathbf{r})$ is a non-negative and normalized boxcar window function so that $\int d^d r G(\mathbf{r}) = 1$, the field $f(\mathbf{x}, t)$ is filtered at scale ℓ as

$$\bar{f}_\ell(\mathbf{x}, t) = \int d^d r G_\ell(\mathbf{r}) f(\mathbf{x} + \mathbf{r}, t).$$

The low-pass filtered $\bar{f}_\ell(\mathbf{x}, t)$ only contains information at length scales $\geq \ell$. The Favre-filtered (density-weighted-filtered) field (Favre 1969) is defined as

$$\tilde{f}_\ell = \bar{\rho} \bar{f}_\ell / \bar{\rho}_\ell$$

We drop the subscript ℓ for notation simplicity. So an overbar \bar{f} denotes a filtered quantity and a tilde \tilde{f} denotes a density-weighted (Favre) filtered quantity.

Proceeding with the Vlasov-Maxwell equations, the resolved kinetic and electromagnetic energy equations at scale ℓ (Matthaeus et al. 2020; Yang et al. 2017a; Eyink 2018) are

$$\partial_t \tilde{E}_\alpha^f + \nabla \cdot \mathbf{J}_\alpha^u = -\Pi_\alpha^{uu} - \Phi_\alpha^{uT} - \Lambda_\alpha^{ub}, \quad (5)$$

$$\partial_t \bar{E}^m + \nabla \cdot \mathbf{J}^b = -\sum_\alpha \Pi_\alpha^{bb} + \sum_\alpha \Lambda_\alpha^{ub}, \quad (6)$$

where $\tilde{E}_\alpha^f = \frac{1}{2} \bar{\rho}_\alpha \tilde{\mathbf{u}}_\alpha^2$ is the filtered fluid flow energy; $\bar{E}^m = (\bar{\mathbf{B}}^2 + \bar{\mathbf{E}}^2)/(8\pi)$ is the filtered electromagnetic energy; $\mathbf{J}_\alpha^u = \tilde{E}_\alpha^f \tilde{\mathbf{u}}_\alpha + \bar{\rho}_\alpha \tilde{\boldsymbol{\tau}}_\alpha^u \cdot \tilde{\mathbf{u}}_\alpha + \bar{\mathbf{P}}_\alpha \cdot \tilde{\mathbf{u}}_\alpha$ and $\mathbf{J}^b = (c\bar{\mathbf{E}} \times \bar{\mathbf{B}})/(4\pi)$ are the spatial transport; $\Pi_\alpha^{uu} = -(\bar{\rho}_\alpha \tilde{\boldsymbol{\tau}}_\alpha^u \cdot \nabla) \cdot \tilde{\mathbf{u}}_\alpha - q_\alpha/c\bar{n}_\alpha \tilde{\boldsymbol{\tau}}_\alpha^b \cdot \tilde{\mathbf{u}}_\alpha$ is the sub-grid-scale (SGS) flux of fluid flow energy across scales due to nonlinearities, where $\tilde{\boldsymbol{\tau}}_\alpha^u = \widetilde{\mathbf{u}_\alpha \mathbf{u}_\alpha} - \tilde{\mathbf{u}}_\alpha \tilde{\mathbf{u}}_\alpha$, $\tilde{\boldsymbol{\tau}}_\alpha^b = \widetilde{\mathbf{u}_\alpha \times \mathbf{B}} - \tilde{\mathbf{u}}_\alpha \times \tilde{\mathbf{B}}$; $\Pi_\alpha^{bb} = -q_\alpha \bar{n}_\alpha \tilde{\boldsymbol{\tau}}_\alpha^e \cdot \tilde{\mathbf{u}}_\alpha$ is the as the SGS flux of electromagnetic energy across scales due to nonlinearities, where $\tilde{\boldsymbol{\tau}}_\alpha^e = \tilde{\mathbf{E}} - \bar{\mathbf{E}}$; $\Phi_\alpha^{uT} = -(\bar{\mathbf{P}}_\alpha \cdot \nabla) \cdot \tilde{\mathbf{u}}_\alpha$ is the rate of flow energy converted into internal energy through filtered $-(\mathbf{P}_\alpha \cdot \nabla) \cdot \mathbf{u}_\alpha$; $\Lambda_\alpha^{ub} = -q_\alpha \bar{n}_\alpha \tilde{\mathbf{E}} \cdot \tilde{\mathbf{u}}_\alpha$ is the rate of conversion of fluid flow energy into electromagnetic energy through filtered $-\mathbf{j}_\alpha \cdot \mathbf{E}$.

We can avoid the complication of the interchange between fluid flow and electromagnetic energy and the spatial transport by summing Eqs. 5 and 6 over species and averaging over space, which yields

$$\underbrace{\partial_t \left\langle \sum_\alpha \tilde{E}_\alpha^f + \bar{E}^m \right\rangle}_{T_{f-\epsilon}} = - \underbrace{\left\langle \sum_\alpha (\Pi_\alpha^{uu} + \Pi_\alpha^{bb}) \right\rangle}_{F_f} - \underbrace{\left\langle \sum_\alpha \Phi_\alpha^{uT} \right\rangle}_{D_f}. \quad (7)$$

The spatial transport terms are globally conservative under suitable boundary conditions, e.g., periodic. ϵ is the total dissipation rate. In the absence of an exact expression of dissipation in collisionless plasma simulations, the dissipation rate is computed by $\epsilon = -d\langle\sum_{\alpha} E_{\alpha}^f + E^m\rangle/dt$. The first term is the time-rate-of-change of energy at scales $\geq \ell$, which is 0 at large enough ℓ and $-\epsilon$ at $\ell \rightarrow 0$. In analogy with the structure function representation in Sec. 2.3, the first term is written as $T_f = \epsilon + \partial_t\langle\sum_{\alpha}\tilde{E}_{\alpha}^f + \bar{E}^m\rangle$, which is the time-rate-of-change of energy at scales $< \ell$ and equals to ϵ at large enough ℓ (e.g., larger than energy-containing scales) and 0 at $\ell \rightarrow 0$. The remaining terms are the nonlinear cross-scale energy flux F_f and the deposition of internal energy received from the cascade D_f . Similar to Eq. 4, the filtered pressure-strain interaction is decomposed as

$$\langle\Phi_{\alpha}^{uT}\rangle = \langle -(\bar{\mathbf{P}}_{\alpha} \cdot \nabla) \cdot \tilde{\mathbf{u}}_{\alpha} \rangle = \langle -\bar{p}_{\alpha} \nabla \cdot \tilde{\mathbf{u}}_{\alpha} \rangle - \langle \bar{\Pi}_{\alpha} : \tilde{\mathbf{D}}_{\alpha} \rangle = \bar{p}\theta_{\alpha} + \bar{P}i\bar{D}_{\alpha}. \quad (8)$$

2.3. Structure Function Representation

The energy distribution among scales can also be defined by considering two-point correlations or the related second-order structure functions. We proceed with the incompressible Hall MHD model due to its relative analytical simplicity. The associated von Kármán-Howarth equation (de Kármán & Howarth 1938; Monin & Yaglom 1975; Verdini et al. 2015; Hellinger et al. 2018; Ferrand et al. 2019; Adhikari et al. 2021) in structure function form is

$$\underbrace{\partial_t S(\ell)/4}_{-T_s} + \underbrace{\nabla_{\ell} \cdot [\mathbf{Y}(\ell)/4 + \mathbf{H}(\ell)/8]}_{-F_s} = -\epsilon + \underbrace{D_{\mu}(\ell) + D_{\eta}(\ell)}_{D_s}, \quad (9)$$

where ℓ is the spatial lag, ∇_{ℓ} is the gradient with respect to the lag ℓ , $S(\ell) = \langle \rho(\delta \mathbf{u})^2 \rangle + \langle (\delta \mathbf{B})^2 \rangle$ is a second-order structure function, \mathbf{u} the bulk fluid velocity, and $\delta \mathbf{u} = \mathbf{u}(\mathbf{x} + \ell) - \mathbf{u}(\mathbf{x})$ defines the increment. $\mathbf{Y}(\ell) = \langle (\delta \mathbf{u})^2 \delta \mathbf{u} + (\delta \mathbf{B})^2 \delta \mathbf{u} - 2(\delta \mathbf{B} \cdot \delta \mathbf{u}) \delta \mathbf{B} \rangle$ is a third-order structure function, $\mathbf{H}(\ell) = \langle 2(\delta \mathbf{B} \cdot \delta \mathbf{j}) \delta \mathbf{B} - (\delta \mathbf{B})^2 \delta \mathbf{j} \rangle$ is the Hall term, and $D_{\mu}(\ell) = \mu \nabla_{\ell}^2 \langle (\delta \mathbf{u})^2 \rangle / 2$ and $D_{\eta}(\ell) = \eta \nabla_{\ell}^2 \langle (\delta \mathbf{B})^2 \rangle / 2$ are the viscous and resistive terms, respectively.

Several points concerning Eq. 9 warrant clarification. First, the terms in Eq. 9 are functions of lag vector (ℓ_x, ℓ_y, ℓ_z) . Upon averaging over directions, the terms in Eq. 9 only depend on lag length ℓ and T_s , F_s and D_s denote omnidirectional forms of the three terms in Eq. 9. Second, Eq. 9 refers to a fluid model, so $\mathbf{u} = (m_i n_i \mathbf{u}_i + m_e n_e \mathbf{u}_e) / (m_i n_i + m_e n_e)$ and $\rho = m_i n_i + m_e n_e$ are dominated by contributions from ions. Third, for the incompressible model used here, we neglect the spatial and time variability of density and set it to be a constant that equals to the spatially and temporally averaged density. The kinetic plasma simulations used here are weakly compressed, which are shown in detail in Sec. 4 and Sec. 5. The incompressible model therefore remains a credible approximation for our simulations. For strongly compressed plasmas, e.g., the turbulent magnetosheath, more elaborate compressive models (Banerjee & Galtier 2013; Hadid et al. 2017; Andrés et al. 2019) are required. Next, the interpretation of $S/4$ is that it is related to the energy at scales $< \ell$. To see this, let the lag $\ell \rightarrow 0$, so that $S/4$ tends to zero, while it equals to the fluid flow and magnetic energy at large ℓ . The second term F_s measures the energy flux through the surface of a lag sphere of radius ℓ . Finally, the viscous and resistive term D_s has the property that for incompressible MHD, it converges to the dissipation rate $\epsilon = \mu \langle \nabla \mathbf{u} : \nabla \mathbf{u} \rangle + \eta \langle \nabla \mathbf{b} : \nabla \mathbf{b} \rangle$ in the limit $\ell \rightarrow 0$. Since this study proceeds with kinetic plasma simulations, we cannot compute ϵ and D_s directly, which instead are derived by $\epsilon = -d\langle\sum_{\alpha} E_{\alpha}^f + E^m\rangle/dt$ and $D_s = \epsilon - T_s - F_s$.

2.4. Association with Dissipation Rate Estimates

To appreciate the physical content of the comparisons below, it is necessary to understand both the differences and the similarities of the energy balance Equations 1-3, the scale filtering formulation Eq. 7 and the structure function formulation Eq. 9, and their associations with dissipation rate. The energy balance equations show direct causality between the global evolutions of energies and $\mathbf{j}_\alpha \cdot \mathbf{E}$ and $-(\mathbf{P}_\alpha \cdot \nabla) \cdot \mathbf{u}_\alpha$, while the scale filtering and structure function formulations show details of energy distributions and dissipation proxies across scales.

The scale filter as implemented in Eq. 7 contains the scale-decomposed energy budget of the full Vlasov Maxwell model. This includes compressive and wave particle effects and contributions from both protons and electrons. The structure function model as implemented in Eq. 9 is a purely fluid construct (incompressible Hall MHD). As such it lacks compressible effects, wave-particle interactions, and other non-Hall kinetic effects. Therefore, we anticipate that the correspondence between Eqs. 7 and 9 may remain credible at MHD scales, identified tentatively as scales larger than ion inertial length.

Even still, the scale-decomposed formulations share common elements in the physics they represent. Both are expressions of conservation of energy across scales and are composed of (i) the rate of change of energy at scales $< \ell$, T_f and T_s ; (ii) energy transfer across scale ℓ , F_f and F_s , leading to the possibility of an inertial range; and (iii) measures of energy dissipation, D_f and D_s . These elements are in direct association with energy dissipation proxies based on the energy transfer process. For example, the time derivative terms T_f and T_s at energy-containing ℓ represent the energy decay rate, which can be taken as a dissipation estimate. According to the von Kármán decay law (Wan et al. 2012a; Wu et al. 2013; Zank et al. 2017; Bandyopadhyay et al. 2018b; Bandyopadhyay et al. 2019),

$$\epsilon_{vK,\pm} = -\frac{d(Z^\pm)^2/2}{dt} = \frac{\alpha_\pm (Z^\pm)^2 Z^\mp}{2 L_\pm}, \quad (10)$$

where α_\pm are positive constants, Z^\pm are the rms fluctuation values of the Elsasser variables, and L_\pm are similarity length scales (correlation lengths are usually used), the energy decay rate is given by $\epsilon_{vK} = (\epsilon_{vK,+} + \epsilon_{vK,-})/2$. The terms F_f and F_s are related to the inertial range energy transfer rate, giving rise to the widely used Yaglom relation (Politano & Pouquet 1998; Sorriso-Valvo et al. 2007; Stawarz et al. 2009; Coburn et al. 2015; Bandyopadhyay et al. 2018; Verdini et al. 2015)

$$\epsilon_{Ym} = -\nabla_\ell \cdot \left(\frac{\mathbf{Y}}{4} + \frac{\mathbf{H}}{8} \right), \quad (11)$$

which can be taken as a dissipation estimate. Although the exact expression of D_s is not known in our kinetic plasma simulations, the term D_f shown in Eq. 7 is the spatial average of filtered pressure-strain interaction, which can estimate the fluid flow energy conversion into internal energy.

In summary, the intent of energy balance equations in Sec. 2.1 is to illuminate global behaviors, while the scale filtering and structure function representations in Sec. 2.2 and Sec. 2.3 aim at scale dependence. Detailed treatments based on the three aforementioned formulations are useful to describe the extent to which these dissipation proxies are correlated and their domain of validity.

3. KINETIC SIMULATIONS: 2.5D AND 3D

Vlasov-Maxwell solutions are obtained with particle in cell (PIC) codes; for run parameters, see Table 1. Here we make use of 2.5 dimensional (2.5D) and 3D kinetic simulations with no external drive. So both are decaying initial value problems.

The 2.5D case was performed using the code P3D (Zeiler et al. 2002) in a 2.5D geometry with turbulent fluctuations in (x, y) plane but no variation in the z direction. All physical quantities have all three components of the vectors. The simulation was performed in a periodic domain, whose size is $L \simeq 150d_i$, where d_i is the ion inertial length, with 4096^2 grid points and 3200 particles of each species per cell ($\sim 1.07 \times 10^{11}$ total particles). The ion-to-electron mass ratio is $m_i/m_e = 25$, and the ratio $\omega_{pe}/\omega_{ce} = 3$, where ω_{pe} is the electron plasma frequency and ω_{ce} is the electron cyclotron frequency. The run was started with uniform density $n_0 = 1.0$ and Maxwellian-distributed ions and electrons with temperature $T_0 = 0.3$. The uniform magnetic field is $B_0 = 1.0$ directed out of the plane, and plasma $\beta = 0.6$. The velocity and magnetic perturbations are transverse to B_0 , typical of “Alfvénic” modes. They were seeded at time $t = 0$ by populating Fourier modes for a range of wavenumbers $2 \leq |\mathbf{k}| \leq 4$ with random phased fluctuations and a specific spectrum. The run was evolved for more than $300\omega_{ci}^{-1}$. This simulation was also used in (Parashar et al. 2018; Yang et al. 2019; Matthaeus et al. 2020; Bandyopadhyay et al. 2021).

The 3D case was obtained using the VPIC code (Bowers et al. 2008). The simulation was conducted in a fully periodic 3D domain of size $L \simeq 42d_i$ with resolution of 2048^3 cells and 150 particles per cell per species ($\sim 2.6 \times 10^{12}$ total particles). The ion-to-electron mass ratio is $m_i/m_e = 50$ and the ratio $\omega_{pe}/\omega_{ce} = 2$. The initial conditions correspond to uniform plasma with density n_0 , Maxwellian-distributed ions and electrons of equal temperature T_0 , uniform magnetic field B_0 in z direction, and plasma $\beta = 0.5$. Turbulent fluctuations were seeded at time $t = 0$ by imposing a large-scale isotropic spectrum of velocity and magnetic fluctuations having polarizations transverse to the guide magnetic field B_0 . The run was evolved for about $170\omega_{ci}^{-1}$. Further details of this simulation can be found in (Roytershteyn et al. 2014).

Dimension	$L(d_i)$	N	m_i/m_e	$B_0\hat{z}$	$\delta b/B_0$	β	ppg
2.5D	150	4096	25	1.0	0.5	0.6	3200
3D	42	2048	50	0.5	1.0	0.5	150

Table 1. 2.5D and 3D PIC simulation parameters: domain size L ; grid points in each direction N ; ion-to-electron mass ratio m_i/m_e ; guide magnetic field in z -direction B_0 ; initial magnetic fluctuation amplitude δb ; plasma β ; average number of particles of each species per grid ppg .

4. GLOBAL BEHAVIOR OF PRESSURE-STRAIN INTERACTION

We study the time evolution of global volume averages of energy to find the electromagnetic work $\langle \mathbf{j}_\alpha \cdot \mathbf{E} \rangle$ versus the pressure-strain interaction $\langle -(\mathbf{P}_\alpha \cdot \nabla) \cdot \mathbf{u}_\alpha \rangle$, the incompressive PiD_α versus compressive $p\theta_\alpha$ conversion of energy, and ion ($\alpha = i$) versus electron ($\alpha = e$) heating. Accurate integrals of energy transfer pathways over time require small time steps and this time-integrated procedure is rather expensive for the 3D PIC simulation. Therefore, the analysis in this section is only conducted using the 2.5D PIC simulation.

Fig. 1 shows the global energy balance by tracking time evolution of the electromagnetic energy $\langle E^m \rangle$, the fluid flow energy of each species $\langle E_\alpha^f \rangle$, and the internal energy of each species $\langle E_\alpha^{th} \rangle$. The total energy $\langle E_{tot} \rangle = \langle E^m + E_i^f + E_e^f + E_i^{th} + E_e^{th} \rangle$ is well conserved, indicating the validity of this

simulation. Note that the electrons gain slightly more internal energy compared to the ions. The stronger electron energization is in conflict with the findings of (Cranmer et al. 2009; Bandyopadhyay et al. 2020a; Hughes et al. 2014) which favor stronger ion heating, while this is consistent with what is observed in (Bandyopadhyay et al. 2021) who found stronger electron heating in turbulent magnetic reconnection. As suggested in early studies, the partitioning of heating between ions and electrons depends on turbulence amplitude (Wu et al. 2013; Matthaeus et al. 2016; Hughes et al. 2017) and plasma β (Howes 2010; Parashar et al. 2018; Vech et al. 2017).

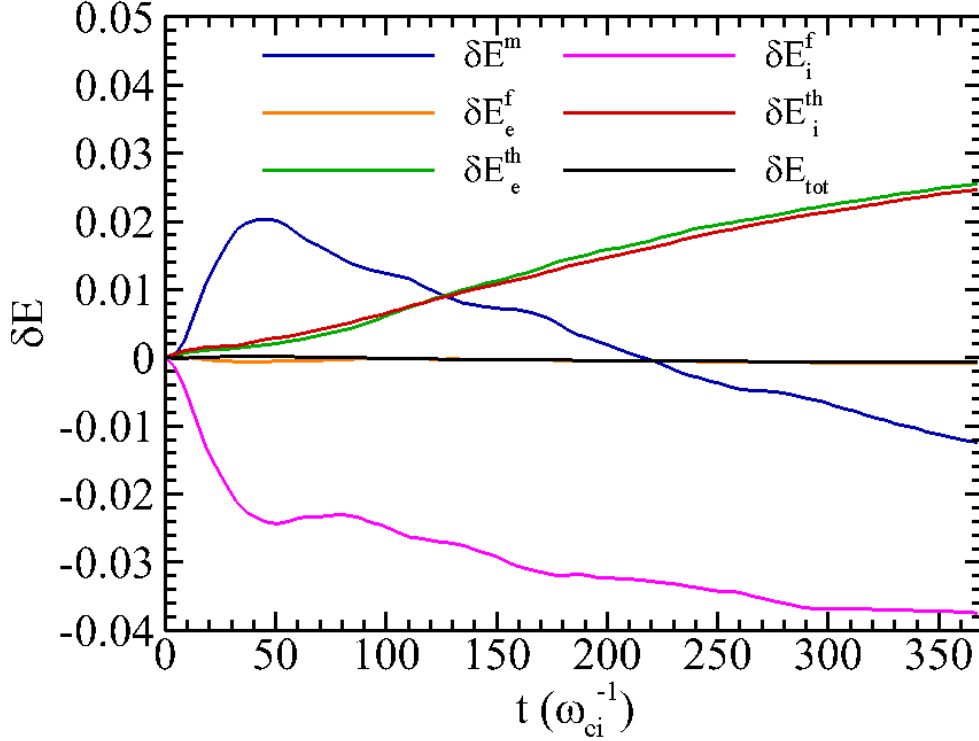


Figure 1. Time evolution of the electromagnetic energy $\langle E^m \rangle$, the fluid flow energy of each species $\langle E_\alpha^f \rangle$, and the internal energy of each species $\langle E_\alpha^{th} \rangle$ for the 2.5D simulation. The change of energy is defined as $\delta E(t) = E(t) - E(0)$. The change of the total energy $\langle E_{tot} \rangle = \langle E^m + E_i^f + E_e^f + E_i^{th} + E_e^{th} \rangle$ is also shown to verify excellent energy conservation.

From Eqs. 1-3, two pathways, the electric work $\langle \mathbf{j}_\alpha \cdot \mathbf{E} \rangle$ and the pressure-strain interaction $\langle -(\mathbf{P}_\alpha \cdot \nabla) \cdot \mathbf{u}_\alpha \rangle$, contribute to the global energy exchange between forms. Their time histories are shown in Fig. 2. One can observe that the global average of the electric work of each species $\langle \mathbf{j}_\alpha \cdot \mathbf{E} \rangle$ in Fig. 2(a) and (b) oscillates significantly over time at high frequencies. This is likely an artefact of the artificial value of ω_{pe}/ω_{ce} in our simulation, and may be remedied by time averaging the results over a plasma oscillation period (Haggerty et al. 2017). The global average of the pressure dilatation of each species $p\theta_\alpha$ in Fig. 2 (c) and (d) also exhibits oscillations, which is attributable to the compression arising from acoustic waves. Since the run we use here is weakly compressible, the incompressible channel PiD_α is favored obviously over the compressive channel $p\theta_\alpha$ for both ions and electrons. Therefore, the global average of the pressure-strain interaction of each species $\langle -(\mathbf{P}_\alpha \cdot \nabla) \cdot \mathbf{u}_\alpha \rangle$ mainly results from the incompressible part PiD_α . However, we cannot rule

out the possibility of stronger $p\theta_\alpha$ at some locations. For example, as shown in the magnetosheath (Chasapis et al. 2018b), the turbulent current sheet (Pezzi et al. 2020; Bandyopadhyay et al. 2021) and the electron diffusion region (Zhou et al. 2021), the local compressive part could dominate over the local incompressible part. Note that there is one peak with magnitude much larger than others in the beginning at $t = 4.5\omega_{ci}^{-1}$. This is due to the initial negligible electric field which responds quickly to obey a solution of the Vlasov-Maxwell system.

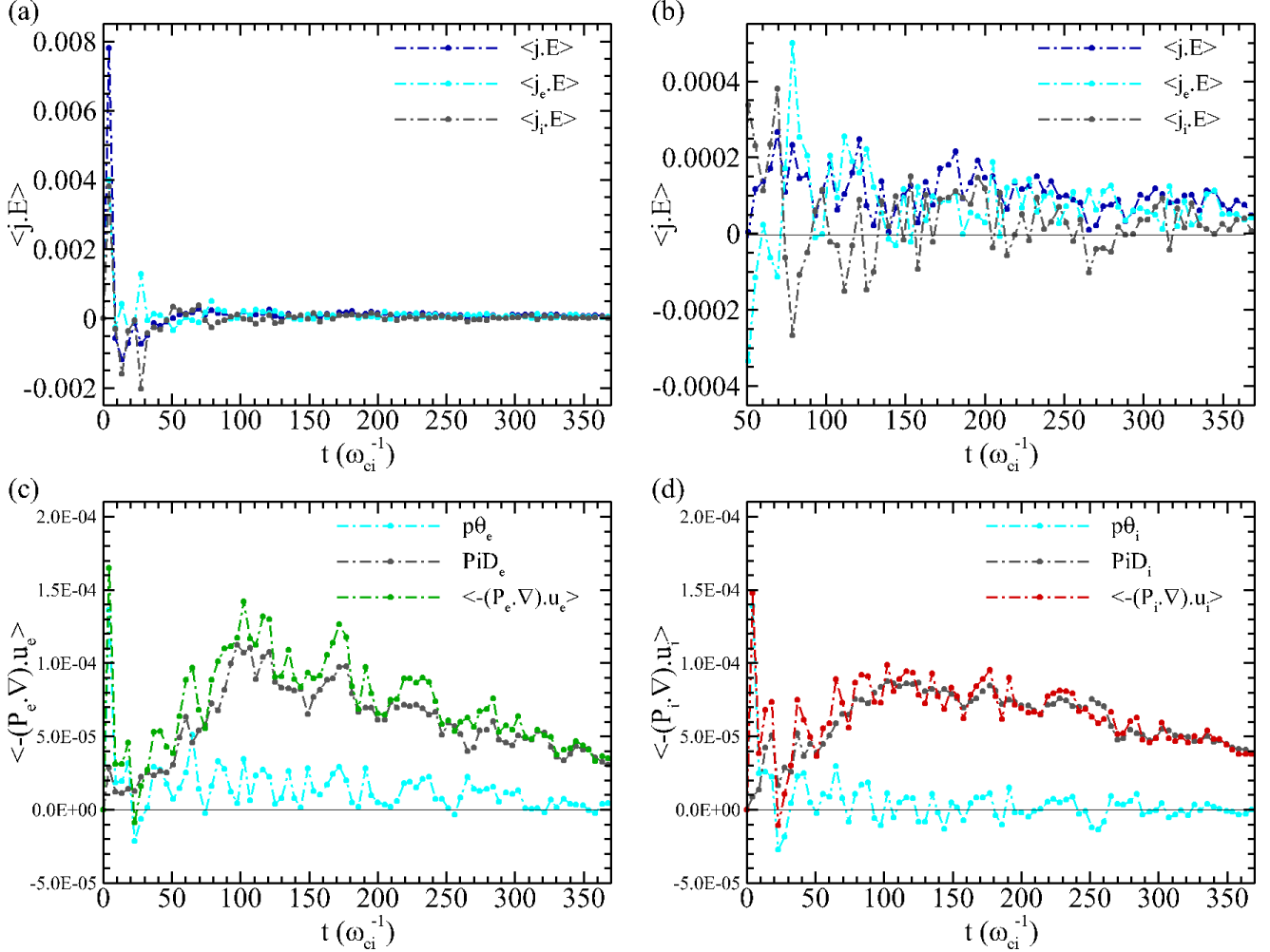


Figure 2. Time evolution of (a) $\langle \mathbf{j}_i \cdot \mathbf{E} \rangle$, $\langle \mathbf{j}_e \cdot \mathbf{E} \rangle$ and $\langle \mathbf{j} \cdot \mathbf{E} \rangle$; (b) zoomed-in electric work showing oscillations; (c) $p\theta_e$, PiD_e , and $\langle -(\mathbf{P}_e \cdot \nabla) \cdot \mathbf{u}_e \rangle$; and (d) $p\theta_i$, PiD_i , and $\langle -(\mathbf{P}_i \cdot \nabla) \cdot \mathbf{u}_i \rangle$ for the 2.5D simulation.

Global energy balance in Eqs. 1-3 is shown in Fig. 3, where the changes of energies contrast with the cumulative time-integrated pathways. These integrals have been numerically computed through the trapezoidal rule and over time interval $[9\omega_{ci}^{-1}, t]$ to avoid the effect of the peaks at $t = 4.5\omega_{ci}^{-1}$ shown in Fig. 2. According to Eq. 2, the internal energy variation of species α , δE_α^{th} , should be equal to the cumulative integral of $\langle -(\mathbf{P}_\alpha \cdot \nabla) \cdot \mathbf{u}_\alpha \rangle$, which is confirmed in Fig. 3. One can see that the cumulative time integrated $\langle -(\mathbf{P}_\alpha \cdot \nabla) \cdot \mathbf{u}_\alpha \rangle$ is almost superposed on the change of internal energy for both electrons and ions. The slight difference mainly results from the level of accuracy of the energy conservation recovered in the simulation and the numerical error of time integration.

As expected from Eq. 3, the cumulative time integrated $\langle -\mathbf{j} \cdot \mathbf{E} \rangle$ is in good agreement with the change of the electromagnetic energy, δE^m . This adds evidence to the idea that despite being adopted widely to estimate heating rate, the electric work $\langle \mathbf{j} \cdot \mathbf{E} \rangle$ is not in direct association with either the internal energy increase or the temperature enhancement. Instead, the change of the internal energy takes place directly through the pressure-strain interaction, $\langle -(\mathbf{P}_\alpha \cdot \nabla) \cdot \mathbf{u}_\alpha \rangle$, for both ions and electrons.

Further examining Fig. 3, we see that the change of the fluid flow energy δE_α^f shows similar trends to the cumulative $\langle \mathbf{j}_\alpha \cdot \mathbf{E} + (\mathbf{P}_\alpha \cdot \nabla) \cdot \mathbf{u}_\alpha \rangle$, in accord with Eq. 1. The non-negligible offsets of the two curves arise in large part from the cumulative numerical error associated with the high frequency oscillations in $\langle \mathbf{j}_\alpha \cdot \mathbf{E} \rangle$ shown in Fig. 2.

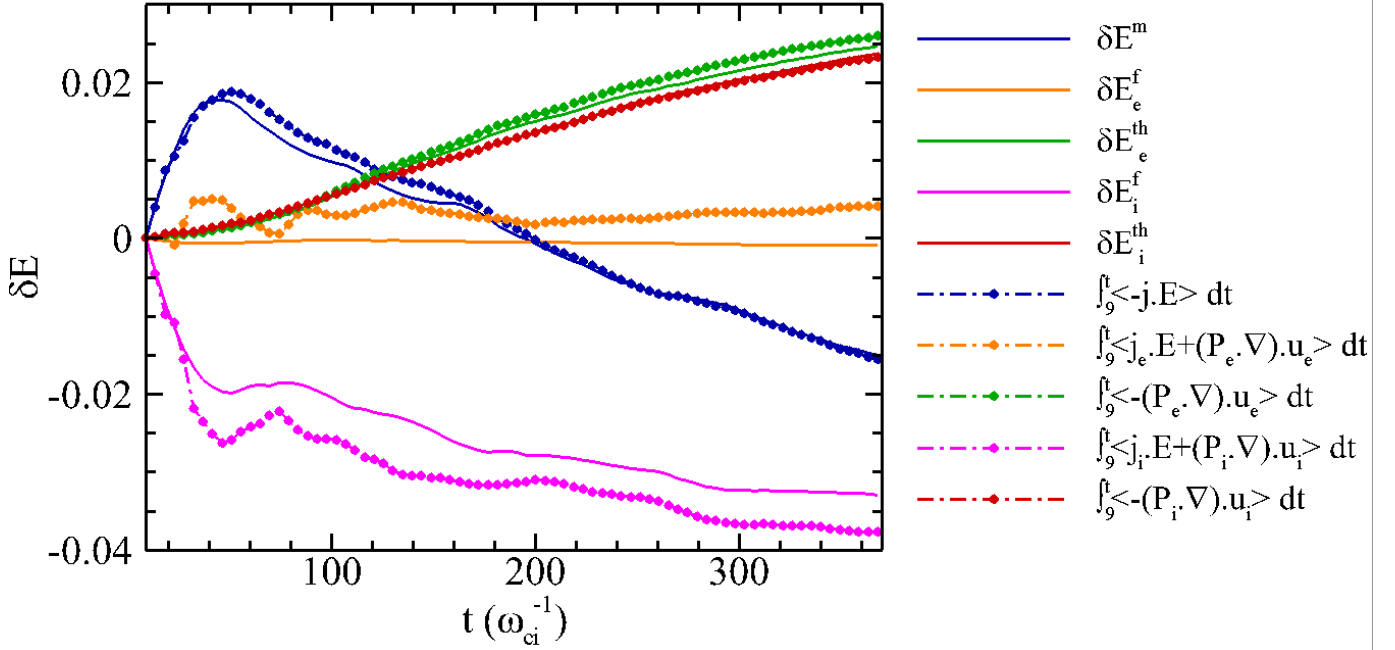


Figure 3. Time evolution of the changes of energies versus cumulative time-integrated $\langle -\mathbf{j} \cdot \mathbf{E} \rangle$, $\langle -(\mathbf{P}_e \cdot \nabla) \cdot \mathbf{u}_e \rangle$, $\langle -(\mathbf{P}_i \cdot \nabla) \cdot \mathbf{u}_i \rangle$, $\langle \mathbf{j}_e \cdot \mathbf{E} + (\mathbf{P}_e \cdot \nabla) \cdot \mathbf{u}_e \rangle$, and $\langle \mathbf{j}_i \cdot \mathbf{E} + (\mathbf{P}_i \cdot \nabla) \cdot \mathbf{u}_i \rangle$ for the 2.5D simulation. Here the change of energy is defined as $\delta E(t) = E(t) - E(9\omega_{ci}^{-1})$ and the cumulative integral is computed over time $[9\omega_{ci}^{-1}, t]$.

5. ENERGY BALANCE ACROSS SCALES

The preceding section investigates global properties of energy conversion in detail. Another important property of plasma turbulence is that it encompasses a vast range of scales. Therefore justification for the identification of relevant dissipation proxies at different scales is crucial. Two simple but essential approaches to resolve or decompose turbulent fields over varying scales are the scale filtering technique, and structure function technique, which give rise to Eq. 7 and Eq. 9, respectively.

To proceed numerically using Eq. 9, the term $\partial_t S(\ell)/4$ is computed by $(S(\ell, t + \Delta t) - S(\ell, t)) / \Delta t$. The gradient ∇_ℓ is computed in lag (ℓ_x, ℓ_y) space spanning $[0, 75d_i] \times [0, 75d_i]$ with 256^2 mesh points in the 2.5D case, and in lag (ℓ_x, ℓ_y, ℓ_z) space spanning $[0, 21d_i] \times [0, 21d_i] \times [0, 21d_i]$ with 64^3 mesh

points in the 3D case. To extract the lag length dependence, we apply directional averaging to obtain lag-length-dependent versions of the quantities T_s , F_s and D_s .

The analysis procedure selects a time shortly after the mean square current density reaches its maximum, by which time the turbulence is fully established. We use 4 time snapshots (i.e., $t = 97.5\omega_{ci}^{-1}$, $102.5\omega_{ci}^{-1}$, $107\omega_{ci}^{-1}$, $111.5\omega_{ci}^{-1}$) in the 2.5D case and 2 time snapshots (i.e., $t = 45\omega_{ci}^{-1}$, $50\omega_{ci}^{-1}$) in the 3D case. These snapshots are separated by time lag $\Delta t \sim 5\omega_{ci}^{-1}$. All following results are averaged over these time snapshots. Fig. 4 shows magnetic energy spectra for the 2.5D case at $t = 97.5\omega_{ci}^{-1}$ and the 3D case at $t = 45\omega_{ci}^{-1}$, where $k^{-5/3}$ and $k^{-8/3}$ power laws are shown for reference in the range $k < 1/d_i$ and $1/d_i < k < 1/d_e$, respectively.

In comparison to the 2.5D simulation, the setup of the 3D kinetic simulation is less than optimal, for example in its relatively small domain size. The expectation follows that for the 3D case the interval of MHD inertial scales will be more limited and not well separated from the injection scale. The spectra are characterized with an upturn at high wavenumbers, which is a cumulative effect of the discrete particle noise inherent in the PIC algorithm. Prior to analysis, we remove noise by low-pass Fourier filter with a cut-off at $kd_i \sim 13$ for the 2.5D case and $kd_i \sim 21$ for the 3D case. This corresponds to filter scales $\ell = \pi/k \sim 0.25d_i$ and $\ell \sim 0.15d_i$, respectively. This filtering procedure has a negligible effect on the following results at scales larger than the cut-off.

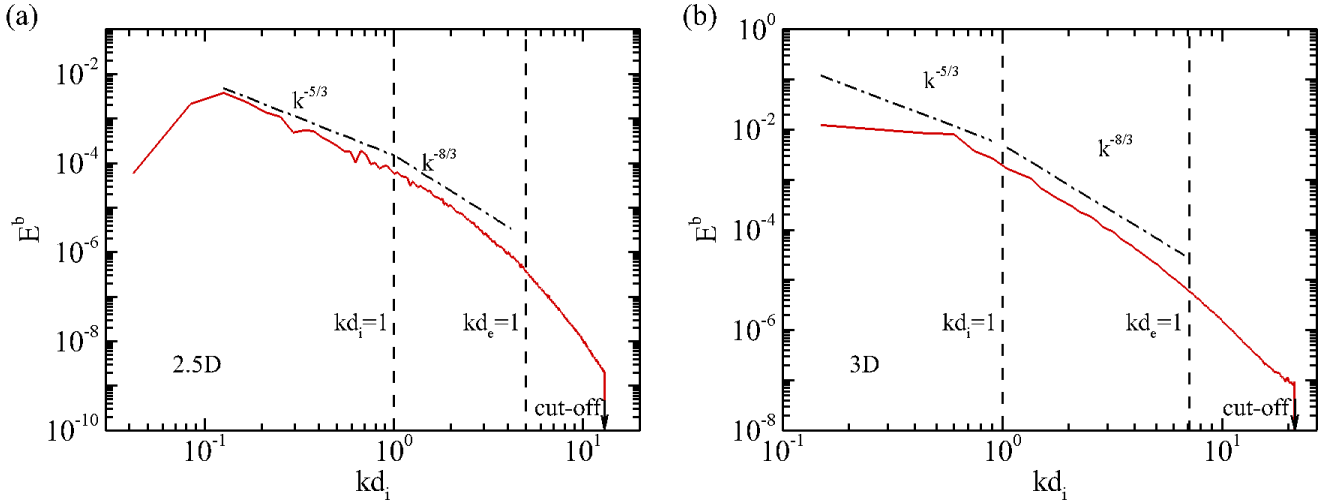


Figure 4. Omnidirectional energy spectra of magnetic fluctuations in 2.5D ($t = 97.5\omega_{ci}^{-1}$) and 3D ($t = 45\omega_{ci}^{-1}$) PIC simulations. Power laws are shown for reference. Vertical lines correspond to ion and electron inertial scales. Filter cut-off is indicated by arrows, as explained in the text.

Analysis of the 2.5D case begins with a scale-filtering description of energy balance in Eq. 7, shown in Fig. 5. The filter cut-off is $\ell = 0.25d_i \sim d_e$ and the correlation length is $\ell \sim 14d_i$, which are indicated by arrows in Fig. 5. The $k^{-5/3}$ power law spectrum in Fig. 4(a) gives a rough suggestion of an MHD inertial range, in the vicinity of a few d_i . One can see that the time derivative term T_f , which is the time rate of change of the cumulative energy in fluctuations at scales $< \ell$, reaches the total dissipation rate ϵ at scales larger than the correlation length, and decreases at intermediate scales (roughly the MHD inertial range), where the nonlinear transfer term F_f sets in and reaches a peak value. The plateau (or, peak) of F_f deviates slightly from ϵ due to the onset of pressure-strain

interaction D_f , which is not negligible at the scale of peak F_f , and which increases towards ϵ at scales much smaller than d_i .

A similar balance holds for the structure function representation in Eq. 9. In this case, the dissipative term D_s , important at small scales, is computed through $D_\mu + D_\eta = \epsilon + \partial_t S/4 + \nabla_r \cdot (\mathbf{Y}/4 + \mathbf{H}/8)$. Again, the Yaglom flux F_s , representing energy transfer by turbulence, reaches a plateau over the intermediate (inertial) scales, at values approaching the system dissipation rate ϵ . The time derivative term T_s saturates to $\sim \epsilon$ at very large scales.

From Fig. 5, we observe the following. First, the scale-by-scale energy budget equation in terms of structure functions (Eq. 9), although shifted slightly, is in good agreement with the analogous expressions in terms of scale filters (Eq. 7). Second, the analogy that exists between the filtered pressure-strain interaction D_f and the dissipative term D_s lends credence to the association of the pressure-strain interaction with the dissipation rate. Finally, the energy loss at energy-containing scales equals the nonlinear energy flux at MHD inertial range and the energy dissipated at kinetic scales. Such a well-distinguished range of scales is indicative of a well-separated inertial range. Accordingly, for cases such as this one, the energy decay rate estimated by the von Kármán decay law in Eq. 10 and the inertial range energy rate estimated by the Yaglom relation in Eq. 11 are reliable proxies of energy dissipation rate.

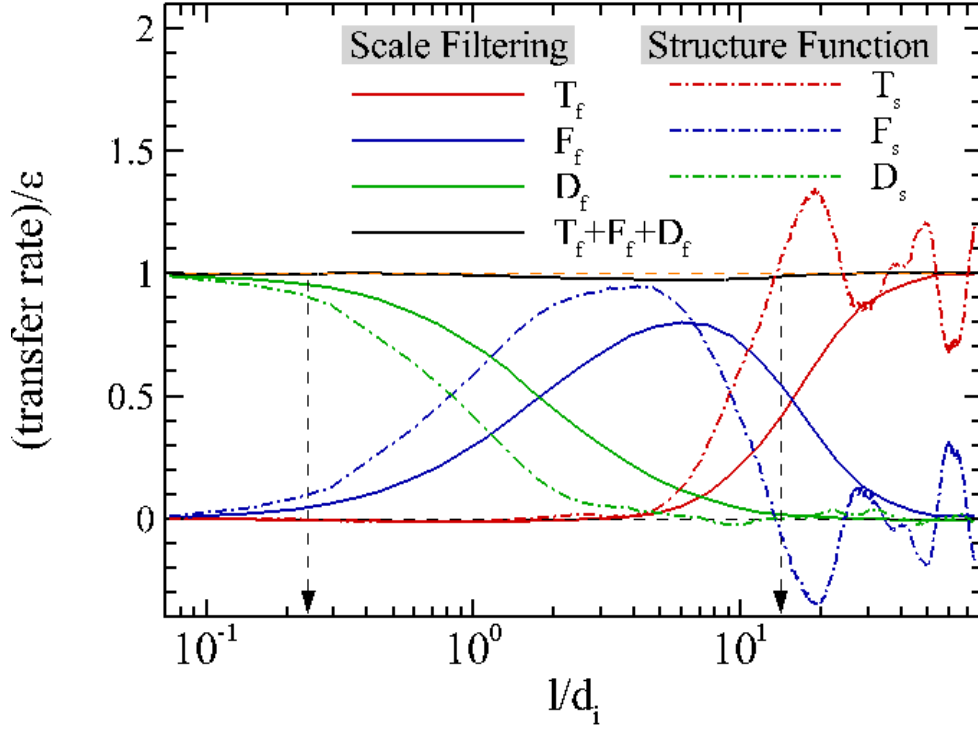


Figure 5. 2.5D PIC result: terms in energy budget equations in terms of scale filters (Eq. 7) and structure functions (Eq. 9) with varying scales. The dissipation rate is computed by $\epsilon = -d \langle \sum_\alpha E_\alpha^f + E^m \rangle / dt$. Vertical dashed lines with arrows indicate filter cut-off and correlation length.

All systems do not necessarily realize a well-defined scale separation as seen in the 2.5D case shown above, see for example the observational result in (Bandyopadhyay et al. 2020; Chhiber et al. 2018).

We use the 3D PIC run, in which scale separation is less well defined, to show how the balance of terms appears in Fig. 6. Most of points made in Fig. 5 remain applicable in Fig. 6, such as the analogy between the scale-filtering and structure function representations, and the similarity between pressure-strain interaction and viscous-resistive effect. In the 3D case (Fig. 6), the dissipation rate is well accounted for by the pressure-strain interaction at kinetic scales and by the time-rate-of-change of filtered energy at energy-containing scales. However, both the nonlinear transfer term F_f and the Yaglom flux F_s saturate to values significantly below ϵ . This is evidently due to the fact that neither the dissipation D_f (D_s) nor the time dependence T_f (T_s) are negligible at those scales.

To obtain a “pure” Yaglom relation (Eq. 11), one requires the existence of the MHD inertial range, in which the dynamics is dominated by inertia terms. It is therefore necessary that the MHD inertial range of scales is (i) at scales small enough that the time-rate-of-change of energy at that scale is negligible, and (ii) at scales large enough that the dissipation at that scale can be neglected. In this sense, the 3D case shown in Fig. 6 manifestly lacks a well-defined scale separation or a well-separated MHD inertial range. This is consistent with the spectrum in Fig. 4(b), but is actually more dramatically illustrated in the analysis shown in the scale decomposition shown in Fig. 6. Consequently, in this 3D case the estimation of dissipation rate based on the Yaglom relation (Eq. 11) falls well below the correct one. Unlike the Yaglom relation, the pressure-strain interaction term traces the conversion of fluid flow energy into internal energy directly, and provides an accurate dissipation rate estimation even in the absence of a well-defined MHD inertial range, as seen in Figs. 5 and 6.

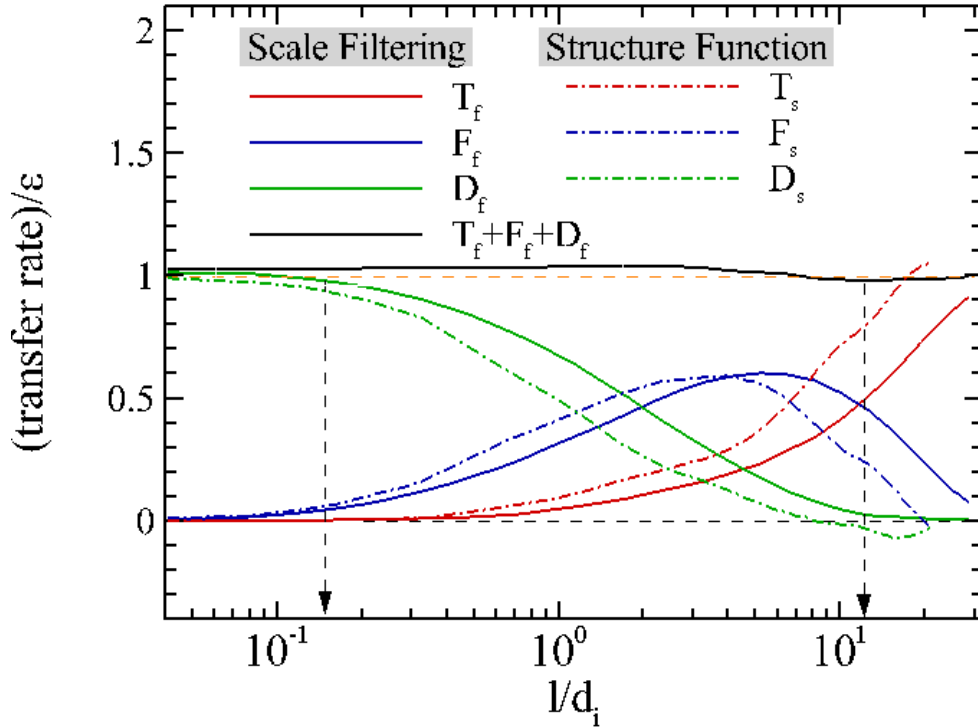


Figure 6. 3D PIC result: the same terms as those in the 2.5D PIC simulation shown in Fig. 5 with varying scales.

As shown in Fig. 2, the compressible part $p\theta_\alpha$ accounts for a very small fraction of the pressure-strain interaction $\langle -(\mathbf{P}_\alpha \cdot \nabla) \cdot \mathbf{u}_\alpha \rangle$ for ions and electrons. In Fig. 7, we show how the compressible $\overline{p\theta_i} + \overline{p\theta_e}$ and incompressible $\overline{PiD_i} + \overline{PiD_e}$ parts in Eq. 8 vary with scales. One can see that the compressible part across scales saturates at kinetic scales, but it is much smaller than the incompressible part for both 2.5D and 3D cases. The compressible part $\overline{p\theta_i} + \overline{p\theta_e}$ for the 3D case is negative, while that for the 2.5D case is positive. One explanation for this sign difference is the oscillatory character of $p\theta_\alpha$ seen in Fig. 2 due to the involvement of acoustic waves.

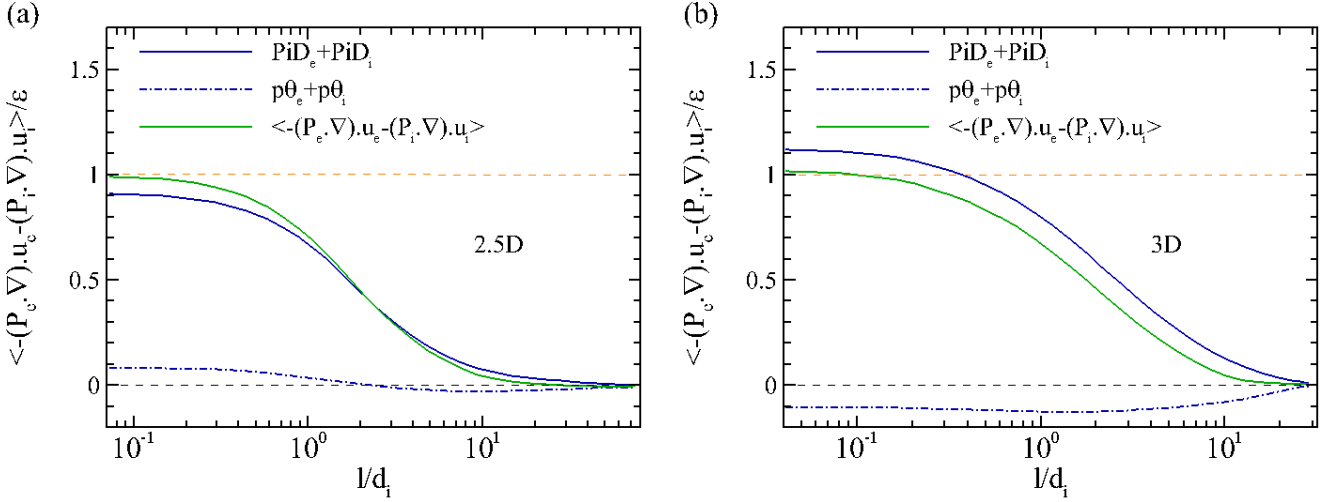


Figure 7. Compressible and incompressible parts in the filtered pressure-strain interaction (Eq. 8) for the 2.5D and 3D PIC simulations.

6. CONCLUSION

The dissipative mechanism in weakly collisional plasma is a topic that pervades decades of studies without a consensus solution. A number of dissipation proxies emerge in the turbulence energy transfer process. In this paper, we study the pressure-strain interaction $-(\mathbf{P}_\alpha \cdot \nabla) \cdot \mathbf{u}_\alpha$ versus other proxies, such as the electromagnetic work $\mathbf{j} \cdot \mathbf{E}$, the energy decay rate ϵ_{vk} from the von Kármán decay law (Wan et al. 2012a; Wu et al. 2013; Zank et al. 2017; Bandyopadhyay et al. 2018b; Bandyopadhyay et al. 2019) and the energy transfer rate ϵ_{Ym} from the Yaglom relation (Politano & Pouquet 1998; Sorriso-Valvo et al. 2007; Stawarz et al. 2009; Coburn et al. 2015; Bandyopadhyay et al. 2018; Verdini et al. 2015). Both the global energy balance and energy budget across scales using the scale filtering and structure function representations¹ are investigated in detail in 2.5D and 3D kinetic simulations.

We confirm that although the electromagnetic work $\mathbf{j} \cdot \mathbf{E}$ has been widely used, the change of the internal energy of each species take places directly through the pressure-strain interaction $-(\mathbf{P}_\alpha \cdot \nabla) \cdot \mathbf{u}_\alpha$. In comparison with the electric work $\mathbf{j} \cdot \mathbf{E}$, the pressure-strain interaction $-(\mathbf{P}_\alpha \cdot \nabla) \cdot \mathbf{u}_\alpha$ has the advantage of tracking electron and ion heating separately. Meanwhile, there can be a correlation between the electromagnetic work and the pressure-strain interaction. For example, from a generalized Ohm's law or the electron momentum equation, in the limit of massless electrons, we can find that $\langle \mathbf{j}_e \cdot \mathbf{E} \rangle = \langle -(\mathbf{P}_e \cdot \nabla) \cdot \mathbf{u}_e \rangle$. No such relation can be obtained for protons.

¹ The guide magnetic field B_0 does not appear explicitly in the scale filtering and structure function representations (Wan et al. 2012a). We expect that both Eqs. 7 and 9 remain applicable in 2D and 3D and even in the presence of guide magnetic field, which is confirmed by checking the energy balance in our 2.5D and 3D kinetic simulations.

The detailed treatment of energy transfer across scales using the scale filtering and structure function representations demonstrates significant caveats present in typical estimations of dissipation based on the von Kármán decay law and the Yaglom relation, while the same analysis shows the advantages of the pressure-strain interaction $\langle -(\mathbf{P}_\alpha \cdot \nabla) \cdot \mathbf{u}_\alpha \rangle$ over other proxies to estimating energy dissipation rate. At energy-containing scales, the time-rate-of-change of energy can be taken as the dissipation rate. However, in real data environment from observations, due to the infeasibility of obtaining the time derivative term, we resort to the von Kármán decay law (Eq. 10) to compute the energy decay rate. This may be inaccurate due to uncertainty of the choices for the similarity lengths L_\pm and the von Kármán constants α_\pm .

In the MHD inertial range of scales, existing studies of energy dissipation in kinetic plasmas have had a particular leaning toward use of the Yaglom relation in observations and simulations. The Yaglom flux ϵ_{Ym} in Eq. 11 is frequently computed or approximated, with only rare attempts made to circumscribe its domain of validity. While we are aware of the important recent developments in deriving Yaglom-like relations for compressible MHD, we have not opted in the present study to implement these theories due to their general complexity, variety of forms and specialization (in some cases) to isothermal turbulence. The incompressive form that we use here evidently remains relevant to our weakly compressible kinetic simulations. Our 2.5D kinetic simulation exhibits a range of scales (inertial range) over which the inertial range energy transfer rate from the Yaglom relation fits well with the real dissipation rate, while observably underestimated inertial range energy transfer rate emerges in our 3D case. This is attributable to the lack of a well-separated inertial range in the 3D kinetic simulation used here. It is worth emphasizing that the Yaglom relation requires that there exists a well-separated inertial range, but well-defined scale separation is not guaranteed a priori. Consequently the prediction that follows from the Yaglom relation should be questionable in the absence of a well-defined inertial range.

In contrast, the pressure-strain interaction $\langle -(\mathbf{P}_\alpha \cdot \nabla) \cdot \mathbf{u}_\alpha \rangle$ turns out to be an accurate estimation of the real dissipation rate even in the absence of a well-defined inertial range. The pressure-strain interaction dominates at kinetic scales d_e , so that deep in the dissipation range, all dissipation is accounted for. One may note that the pressure-strain interaction is also analogous to the viscous-collisional case in the sense that its global average could depend on velocity gradient as well (Vasquez & Markovskii 2012; Del Sarto & Pegoraro 2018; Yang et al. 2017a; Yang et al. 2017a; Parashar et al. 2018).

In principle the pressure-strain interaction $\langle -(\mathbf{P}_\alpha \cdot \nabla) \cdot \mathbf{u}_\alpha \rangle$ is a much more complete representation of dissipation in kinetic plasma in several ways. Firstly, $\langle -(\mathbf{P}_\alpha \cdot \nabla) \cdot \mathbf{u}_\alpha \rangle$ is readily resolved into contributions of electrons and ions (and additional species if present). Therefore this approach is useful to understand the distribution of dissipated energy between different species (Sitnov et al. 2018; Bandyopadhyay et al. 2021). Secondly, $\langle -(\mathbf{P}_\alpha \cdot \nabla) \cdot \mathbf{u}_\alpha \rangle$ includes both compressive and incompressive contributions, while most of other estimates are limited to incompressive contributions. The kinetic simulations used here are weakly compressive, and more samples with stronger compression are required to assess detailed contributions from the compressive part of $\langle -(\mathbf{P}_\alpha \cdot \nabla) \cdot \mathbf{u}_\alpha \rangle$ to the energy dissipation (Chasapis et al. 2018b; Du et al. 2018; Pezzi et al. 2020; Wang et al. 2021; Zhou et al. 2021; Bandyopadhyay et al. 2021). Thirdly, $\langle -(\mathbf{P}_\alpha \cdot \nabla) \cdot \mathbf{u}_\alpha \rangle$ remains applicable to anisotropic cases, in which we can figure out the preferential dissipation direction (Song et al. 2020). Finally, without taking spatial average, $-(\mathbf{P}_\alpha \cdot \nabla) \cdot \mathbf{u}_\alpha$ is spatially localized, which can be applied to examine the

contribution from each point in space and identify sites of heating (Yang et al. 2017b,a; Yang et al. 2019; Pezzi et al. 2019b). We should also keep in mind that the transport terms shown in Eq. 2 are likely to exert significant influence on the values of $-(\mathbf{P}_\alpha \cdot \nabla) \cdot \mathbf{u}_\alpha$ (Du et al. 2020; Fadanelli et al. 2021) actually obtained, and may therefore influence dissipation even if the pressure-strain remains an accurate quantitative measure of the dissipation itself.

ACKNOWLEDGMENTS

This research has been supported by NSFC Grant Nos. 91752201, 11672123 and 11902138, by the US National Science Foundation under NSF-DOE grant PHYS- 2108834, by the NASA Magnetospheric Multiscale mission under NASA grant 80NSSC19K0565, and by NSF/DOE grant DESC0019315 and XSEDE allocation TG-ATM180015. We acknowledge computing support provided by Center for Computational Science and Engineering of Southern University of Science and Technology and the use of Information Technologies (IT) resources at the University of Delaware, specifically the high-performance computing resources.

REFERENCES

- Adhikari, S., Parashar, T., Shay, M., et al. 2021, Physical Review E, 104, 065206
- Aluie, H. 2013, Physica D, 247, 54, doi: [10.1016/j.physd.2012.12.009](https://doi.org/10.1016/j.physd.2012.12.009)
- Andrés, N., Sahraoui, F., Galtier, S., et al. 2019, Phys. Rev. Lett., 123, 245101, doi: [10.1103/PhysRevLett.123.245101](https://doi.org/10.1103/PhysRevLett.123.245101)
- Bandyopadhyay, R., Matthaeus, W. H., Oughton, S., & Wan, M. 2019, Journal of Fluid Mechanics, 876, 5
- Bandyopadhyay, R., Oughton, S., Wan, M., et al. 2018a, Physical Review X, 8, 041052, doi: [10.1103/PhysRevX.8.041052](https://doi.org/10.1103/PhysRevX.8.041052)
- Bandyopadhyay, R., Chasapis, A., Chhiber, R., et al. 2018b, Astrophys. J., 866, 106, doi: [10.3847/1538-4357/aade04](https://doi.org/10.3847/1538-4357/aade04)
- Bandyopadhyay, R., Chasapis, A., Chhiber, R., et al. 2018, arXiv preprint arXiv:1807.06140
- Bandyopadhyay, R., Matthaeus, W. H., Parashar, T. N., et al. 2020a, Phys. Rev. Lett., 124, 255101, doi: [10.1103/PhysRevLett.124.255101](https://doi.org/10.1103/PhysRevLett.124.255101)
- Bandyopadhyay, R., Goldstein, M., Maruca, B., et al. 2020b, The Astrophysical Journal Supplement Series, 246, 48
- Bandyopadhyay, R., Sorriso-Valvo, L., Chasapis, A. r., et al. 2020, Phys Rev. Lett., 124, 225101, doi: [10.1103/PhysRevLett.124.225101](https://doi.org/10.1103/PhysRevLett.124.225101)
- Bandyopadhyay, R., Chasapis, A., Matthaeus, W., et al. 2021, Physics of Plasmas, 28, 112305
- Banerjee, S., & Galtier, S. 2013, Phys. Rev. E, 87, doi: [10.1103/PhysRevE.87.013019](https://doi.org/10.1103/PhysRevE.87.013019)
- Biskamp, D. 2003, Magnetohydrodynamic Turbulence (Cambridge, UK: Cambridge University Press)
- Bowers, K., & Li, H. 2007, Phys. Rev. Lett., 98, doi: [10.1103/PhysRevLett.98.035002](https://doi.org/10.1103/PhysRevLett.98.035002)
- Bowers, K. J., Albright, B. J., Yin, L., Bergen, B., & Kwan, T. J. 2008, Phys.Plasmas, 15, 055703
- Breech, B., Matthaeus, W. H., Minnie, J., et al. 2008, J. Geophys. Res., 113, doi: [10.1029/2007JA012711](https://doi.org/10.1029/2007JA012711)
- Camporeale, E., Sorriso-Valvo, L., Califano, F., & Retinò, A. 2018, Physical review letters, 120, 125101
- Cerri, S., & Camporeale, E. 2020, Physics of Plasmas, 27, 082102
- Chandran, B. D., Li, B., Rogers, B. N., Quataert, E., & Germaschewski, K. 2010, The Astrophysical Journal, 720, 503
- Chasapis, A., Matthaeus, W., Parashar, T., et al. 2018a, The Astrophysical Journal Letters, 856, L19
- Chasapis, A., Yang, Y., Matthaeus, W., et al. 2018b, The Astrophysical Journal Letters, 862
- Chen, C., Klein, K., & Howes, G. G. 2019, Nature communications, 10, 1

- Chhiber, R., Chasapis, A., Bandyopadhyay, R., et al. 2018, *Journal of Geophysical Research (Space Physics)*, 123, 9941, doi: [10.1029/2018JA025768](https://doi.org/10.1029/2018JA025768)
- Coburn, J. T., Forman, M. A., Smith, C. W., Vasquez, B. J., & Stawarz, J. E. 2015, *Phil. Trans. R. Soc. A*, 373, 20140150
- Cranmer, S. R., Matthaeus, W. H., Breech, B. A., & Kasper, J. C. 2009, *Astrophys. J.*, 702, 1604, doi: [10.1088/0004-637X/702/2/1604](https://doi.org/10.1088/0004-637X/702/2/1604)
- de Kármán, T., & Howarth, L. 1938, *Proc. Roy. Soc. London Ser. A*, 164, 192, doi: [10.1098/rspa.1938.0013](https://doi.org/10.1098/rspa.1938.0013)
- Del Sarto, D., & Pegoraro, F. 2018, *Month. Not. Roy. Astron. Soc.*, 475, 181, doi: [10.1093/mnras/stx3083](https://doi.org/10.1093/mnras/stx3083)
- Dmitruk, P., Matthaeus, W. H., & Seenu, N. 2004, *Astrophys. J.*, 617, 667
- Du, S., Guo, F., Zank, G. P., Li, X., & Stanier, A. 2018, *The Astrophysical Journal*, 867, 16
- Du, S., Zank, G. P., Li, X., & Guo, F. 2020, *Physical Review E*, 101, 033208
- Ergun, R., Goodrich, K., Wilder, F., et al. 2018, *Geophysical Research Letters*, 45, 3338
- Eyink, G. L. 2003, *Nonlinearity*, 16, 137, doi: [10.1088/0951-7715/16/1/309](https://doi.org/10.1088/0951-7715/16/1/309)
- Eyink, G. L. 2018, *Physical Review X*, 8, 041020
- Fadanelli, S., Lavraud, B., Califano, F., et al. 2021, *Journal of Geophysical Research: Space Physics*, 126, e2020JA028333
- Favre, A. 1969, *Soc. Indust. Appl. Math.*, 231
- Ferrand, R., Galtier, S., Sahraoui, F., et al. 2019, *The Astrophysical Journal*, 881, 50
- Frisch, U. 1995, *Turbulence. The legacy of A.N. Kolmogorov* (Cambridge U.Press)
- Gary, S. P., & Saito, S. 2003, *J. Geophys. Res.*, 108, 1194
- Gary, S. P., Saito, S., & Li, H. 2008, *Geophys. Res. Lett.*, 35, L02104
- Germano, M. 1992, *Journal of Fluid Mechanics*, 238, 325, doi: [10.1017/S0022112092001733](https://doi.org/10.1017/S0022112092001733)
- Hadid, L., Sahraoui, F., & Galtier, S. 2017, *The Astrophysical Journal*, 838, 9
- Haggerty, C. C., Parashar, T. N., Matthaeus, W. H., et al. 2017, *Physics of Plasmas*, 24, 102308, doi: [10.1063/1.5001722](https://doi.org/10.1063/1.5001722)
- He, J., Wang, L., Tu, C., Marsch, E., & Zong, Q. 2015, *The Astrophysical Journal Letters*, 800, L31
- He, J., Zhu, X., Chen, Y., et al. 2018, *The Astrophysical Journal*, 856, 148
- Hellinger, P., Verdini, A., Landi, S., Franci, L., & Matteini, L. 2018, *The Astrophysical Journal Letters*, 857, L19
- Hollweg, J. V. 1986, *J. Geophys. Res.*, 91, 4111
- Hollweg, J. V., & Isenberg, P. A. 2002, *J. Geophys. Res.*, 107, 1147
- Hossain, M., Gray, P. C., Pontius Jr, D. H., Matthaeus, W. H., & Oughton, S. 1995, *Physics of Fluids*, 7, 2886
- Howes, G., Dorland, W., Cowley, S., et al. 2008, *Physical Review Letters*, 100, 065004
- Howes, G. G. 2010, *Monthly Notices of the Royal Astronomical Society: Letters*, 409, L104
- Howes, G. G., Tenborge, J. M., Dorland, W., et al. 2011, *Phys. Rev. Lett.*, 107, doi: [10.1103/PhysRevLett.107.035004](https://doi.org/10.1103/PhysRevLett.107.035004)
- Hughes, R. S., Gary, S. P., & Wang, J. 2014, *Geophysical Research Letters*, 41, 8681
- Hughes, R. S., Gary, S. P., Wang, J., & Parashar, T. N. 2017, *The Astrophysical Journal Letters*, 847, L14
- Jiang, K., Huang, S., Yuan, Z., et al. 2021, *Geophysical Research Letters*, 48, e2021GL093458
- Klein, K. G., & Howes, G. G. 2016, *The Astrophysical Journal Letters*, 826, L30
- Klein, K. G., Howes, G. G., TenBarge, J. M., & Valentini, F. 2020, *Journal of Plasma Physics*, 86
- Kolmogorov, A. N. 1941a, *Dokl. Akad. Nauk SSSR*, 30, 301, doi: [10.1098/rspa.1991.0075](https://doi.org/10.1098/rspa.1991.0075)
- . 1941b, *C.R. Acad. Sci. U.R.S.S.*, 31, 538
- Liang, H., Cassak, P. A., Servidio, S., et al. 2019, *Physics of Plasmas*, 26, 082903
- Lu, S., Angelopoulos, V., Artemyev, A., et al. 2019, *The Astrophysical Journal*, 878, 109
- Markovskii, S. A., Vasquez, B. J., Smith, C. W., & Hollweg, J. V. 2006, *Astrophys. J.*, 639, 1177
- Matthaeus, W. H., Parashar, T. N., Wan, M., & Wu, P. 2016, *Astrophys. J. Lett.*, 827, L7, doi: [10.3847/2041-8205/827/1/L7](https://doi.org/10.3847/2041-8205/827/1/L7)
- Matthaeus, W. H., Yang, Y., Wan, M., et al. 2020, *Astrophys. J.*, 891, 101, doi: [10.3847/1538-4357/ab6d6a](https://doi.org/10.3847/1538-4357/ab6d6a)
- Meneveau, C., & Katz, J. 2000, *Ann. Rev. Fluid Mech.*, 32, 1

- Moffatt, H. K. 1978, *Magnetic Field Generation in Electrically Conducting Fluids* (New York: Cambridge University Press)
- Monin, A. S., & Yaglom, A. M. 1975, *Statistical Fluid Mechanics*, Vol. 2 (Cambridge, Mass.: MIT Press)
- Osman, K. T., Wan, M., Matthaeus, W. H., Weygand, J. M., & Dasso, S. 2011, *Phys. Rev. Lett.*, 107, 165001
- Parashar, T. N., Matthaeus, W. H., & Shay, M. A. 2018, Accepted for publications in *ApJ Letters*
- Parashar, T. N., Servidio, S., Shay, M. A., Breech, B., & Matthaeus, W. H. 2011, *Phys. Plasmas*, 18, 092302
- Parashar, T. N., Shay, M. A., Cassak, P. A., & Matthaeus, W. H. 2009, *Phys. Plasmas*, 16, doi: [10.1063/1.3094062](https://doi.org/10.1063/1.3094062)
- Parker, E. N. 1979, *Cosmical Magnetic Fields: Their Origin and Activity* (Oxford, UK: Oxford Univeristy Press)
- Perri, S., Goldstein, M. L., Dorelli, J. C., & Sahraoui, F. 2012, *Phys. Rev. Lett.*, 109, 191101
- Pezzi, O., Perrone, D., Servidio, S., et al. 2019a, *apj*, 887, 208, doi: [10.3847/1538-4357/ab5285](https://doi.org/10.3847/1538-4357/ab5285)
- Pezzi, O., Yang, Y., Valentini, F., et al. 2019b, *Physics of Plasmas*, 26, 072301, doi: [10.1063/1.5100125](https://doi.org/10.1063/1.5100125)
- Pezzi, O., Liang, H., Juno, J., et al. 2020, *Monthly Notices of the Royal Astronomical Society*, 505, 4857–4873
- Phan, T., Eastwood, J. P., Shay, M., et al. 2018, *Nature*, 557, 202
- Podesta, J. 2008, *Journal of Fluid Mechanics*, 609, 171
- Politano, H., & Pouquet, A. 1998, *Geophys. Res. Lett.*, 25, 273, doi: [10.1029/97GL03642](https://doi.org/10.1029/97GL03642)
- Pongkitiwanichakul, P., Ruffolo, D., Guo, F., et al. 2021, *The Astrophysical Journal*, 923, 182
- Pope, S. B. 2004, *New J. Phys.*, 6, 35, doi: [10.1088/1367-2630/6/1/035](https://doi.org/10.1088/1367-2630/6/1/035)
- Retinò, A., Sundkvist, D., Vaivads, A., et al. 2007, *Nature Phys.*, 3, 235
- Roytershteyn, V., Karimabadi, H., Uritsky, V. M., et al. 2014, in preparation
- Sitnov, M., Merkin, V., Roytershteyn, V., & Swisdak, M. 2018, *Geophysical Research Letters*, 45, 4639
- Song, L., Zhou, M., Yi, Y., et al. 2020, *Journal of Geophysical Research: Space Physics*, 125, e2020JA028278
- Sorriso-Valvo, L., Marino, R., Carbone, V., et al. 2007, *Phys. Rev. Lett.*, 99, 115001
- Stawarz, J. E., Smith, C. W., Vasquez, B. J., Forman, M. A., & MacBride, B. T. 2009, *Astrophys. J.*, 697, 1119
- Sundkvist, D., Retinò, A., Vaivads, A., & Bale, S. D. 2007, *Phys. Rev. Lett.*, 99, 025004
- Taylor, G. I. 1938, *Proc. Roy. Soc. Lond. A*, 164, 476, doi: [10.1098/rspa.1938.0032](https://doi.org/10.1098/rspa.1938.0032)
- Teaca, B., Gorbunov, E. A., Told, D., Bañón Navarro, A., & Jenko, F. 2021, *Journal of Plasma Physics*, 87, 905870209, doi: [10.1017/S0022377821000180](https://doi.org/10.1017/S0022377821000180)
- TenBarge, J. M., & Howes, G. G. 2013, *Astrophys. J. Lett.*, 771, L27
- Vasquez, B. J., & Markovskii, S. A. 2012, *Astrophys. J.*, 747, 19
- Vech, D., Klein, K. G., & Kasper, J. C. 2017, *The Astrophysical Journal Letters*, 850, L11
- Verdini, A., Grappin, R., Hellinger, P., Landi, S., & Müller, W. C. 2015, *Astrophys. J.*, 804, 119, doi: [10.1088/0004-637X/804/2/119](https://doi.org/10.1088/0004-637X/804/2/119)
- Vörös, Z., Yordanova, E., Khotyaintsev, Y. V., Varsani, A., & Narita, Y. 2019, *Frontiers in Astronomy and Space Sciences*, 6, 60
- Wan, M., Matthaeus, W. H., Roytershteyn, V., et al. 2015, *Phys. Rev. Lett.*, 114, 175002
- Wan, M., Oughton, S., Servidio, S., & Matthaeus, W. H. 2012a, *J. Fluid Mech.*, 697, 296, doi: [10.1017/jfm.2012.61](https://doi.org/10.1017/jfm.2012.61)
- Wan, M., Servidio, S., Oughton, S., & Matthaeus, W. H. 2009, *Physics of plasmas*, 16, 090703
- Wan, M., Matthaeus, W. H., Karimabadi, H., et al. 2012b, *Phys. Rev. Lett.*, 109, 195001
- Wang, Y., Bandyopadhyay, R., Chhiber, R., et al. 2021, *Journal of Geophysical Research (Space Physics)*, 126, e29000, doi: [10.1029/2020JA029000](https://doi.org/10.1029/2020JA029000)
- Wu, P., Wan, M., Matthaeus, W. H., Shay, M. A., & Swisdak, M. 2013, *Phys. Rev. Lett.*, 111, 121105, doi: [10.1103/PhysRevLett.111.121105](https://doi.org/10.1103/PhysRevLett.111.121105)
- Yang, Y. 2019, *Energy transfer and dissipation in plasma turbulence: from compressible mhd to collisionless plasma* (Springer)
- Yang, Y., Wan, M., Matthaeus, W. H., et al. 2019, *Monthly Notices of the Royal Astronomical Society*, 482, 4933
- Yang, Y., Matthaeus, W. H., Parashar, T. N., et al. 2017a, *Physics of Plasmas*, 24, 072306, doi: [10.1063/1.4990421](https://doi.org/10.1063/1.4990421)

- . 2017b, *Phys. Rev. E*, 95, 061201,
doi: [10.1103/PhysRevE.95.061201](https://doi.org/10.1103/PhysRevE.95.061201)
- Yang, Y., Matthaeus, W. H., Parashar, T. N.,
et al. 2017a, *Phys. Rev. E*, 95, 061201
- . 2017b, *Phys. Plasmas*, 24, 072306
- Zank, G. P., Adhikari, L., Hunana, P., et al. 2017,
The Astrophysical Journal, 835, 147,
doi: [10.3847/1538-4357/835/2/147](https://doi.org/10.3847/1538-4357/835/2/147)
- Zeiler, A., Biskamp, D., Drake, J. F., et al. 2002,
J. Geophys. Res., 107, 1230
- Zenitani, S., Hesse, M., Klimas, A., & Kuznetsova,
M. 2011, *Physical review letters*, 106, 195003
- Zhong, Z., Deng, X., Zhou, M., et al. 2019,
Geophysical Research Letters, 46, 12693
- Zhou, M., Man, H., Yang, Y., Zhong, Z., & Deng,
X. 2021, *Geophysical Research Letters*,
e2021GL096372